Title
Halogen-driven low-altitude O3 and hydrocarbon losses in spring at northern high latitudes

Journal
Journal of Geophysical Research, 111(D17)

ISSN
0148-0227

Authors
Zeng, Tao
Wang, Yuhang
Chance, Kelly
et al.

Publication Date
2006

DOI
10.1029/2005jd006706

Halogen-driven low-altitude O_3 and hydrocarbon losses in spring at northern high latitudes

Tao Zeng,[1] Yuhang Wang,[1] Kelly Chance,[2] Nicola Blake,[3] Donald Blake,[3] and Brian Ridley[4]

Received 22 September 2005; revised 13 April 2006; accepted 11 May 2006; published 15 September 2006.

[1] Halogen-driven ozone and hydrocarbon losses in springtime Arctic boundary layer are investigated using a regional chemical transport model. Surface observations of ozone at Alert and Barrow and aircraft observations of ozone and hydrocarbons during the Tropospheric Ozone Production about the Spring Equinox (TOPSE) experiment from February to May in 2000 are analyzed. We prescribe halogen radical distributions on the basis of GOME BrO observations. Tropospheric GOME BrO column shows an apparent anticorrelation with surface temperature over high-BrO regions. The enhancements of tropospheric BrO columns coincide with movements of cold polar air masses. While GOME BrO measurements reach the maximum in March, simulated near-surface ozone loss peaks in April because of the increasing daylight hours and hence the time for chemical processing. At its peak, the area of simulated near-surface ozone depletions (O_3 < 20 ppbv) covers >50% of the northern high latitudes. Analysis of surface measurements at Alert and Barrow points to the importance of long-range transport of ozone-poor air from high-BrO regions. We find that specifying a BrO layer thickness of 300 m results in the best overall agreement between observed and simulated ozone. The apparent halogen-driven ozone loss up to 1 km was reproduced in the model because of vertical transport of ozone-poor air from low altitudes. When the empirical Cl/Br ratios derived from previous observations are used, the model can reproduce the observed halogen loss of light alkanes and acetylene. The Cl/Br ratios from a recent box model study using an accepted chemical mechanism are, however, much higher than the empirical results. We show that the hydrocarbon loss is not as sensitive to the prescribed thickness of the halogen layer as the ozone loss, therefore representing a more robust measure for evaluating satellite BrO column measurements.

Citation: Zeng, T., Y. Wang, K. Chance, N. Blake, D. Blake, and B. Ridley (2006), Halogen-driven low-altitude O_3 and hydrocarbon losses in spring at northern high latitudes, *J. Geophys. Res.*, *111*, D17313, doi:10.1029/2005JD006706.

1. Introduction

[2] Near surface ozone depletion events (ODEs) at northern high latitudes during polar sunrise were first discovered two decades ago [*Oltmans et al.*, 1986; *Bottenheim et al.*, 1986]. Bromine chemistry is believed to be responsible for this unusual phenomenon through the following catalytic cycle [*Barrie et al.*, 1988],

(R1) $$O_3 + Br \rightarrow BrO + O_2$$

(R2) $$BrO + BrO \rightarrow 2Br + O_2$$

In this cycle, the rate-limiting step is reaction (R2), implying that ozone loss chemistry is a quadratic function of BrO concentrations [*Hausmann and Platt*, 1994],

$$\frac{d[O_3]}{dt} = -2k_2[BrO]^2 \quad (1)$$

[3] Suspended sea-salt aerosols [*Barrie et al.*, 1988], deposited sea-salt aerosols on ice/snowpack [*Tang and McConnell*, 1996; *Impey et al.*, 1999], and ice crystals [*McConnell et al.*, 1992] are thought to provide reaction surfaces for generating gaseous halogen species. Two heterogeneous reactions were postulated to be involved in the activations of bromine and chlorine radicals [*Fan and Jacob*, 1992; *Vogt et al.*, 1996; *Foster et al.*, 2001].

(R3) $$HOBr + Br^- + H^+ \rightarrow Br_2 + H_2O$$

(R4) $$HOBr + Cl^- + H^+ \rightarrow BrCl + H_2O$$

[1]School of Earth and Atmospheric Sciences, Georgia Institute of Technology, Atlanta, Georgia, USA.
[2]Harvard-Smithsonian Center for Astrophysics, Cambridge, Massachusetts, USA.
[3]Department of Chemistry, University of California at Irvine, Irvine, California, USA.
[4]Atmospheric Chemistry Division, National Center for Atmospheric Research, Boulder, Colorado, USA.

0148-0227/06/2005JD006706

[4] Several box model studies [*Fan and Jacob*, 1992; *Tang and McConnell*, 1996; *Vogt et al.*, 1996; *Sander and Crutzen*, 1996; *Sander et al.*, 1997; *Michalowski et al.*, 2000; *Evans et al.*, 2003] have investigated polar surface halogen chemistry by incorporating heterogeneous halogen chemical mechanisms. Quantitative evaluations of the heterogeneous halogen sources and the mechanisms remain difficult because of a lack of direct observation of key radical species. Surface and aircraft field measurements clearly indicate the frequent occurrence of near-surface ODEs in the spring Arctic [e.g., *Oltmans et al.*, 1986; *Bottenheim et al.*, 1986; *Anlauf et al.*, 1994; *Atlas et al.*, 2003; *Ridley et al.*, 2003]. Differential Optical Absorption Spectroscopy (DOAS) measurements of BrO showed the close associations of high BrO concentrations and ODEs [e.g., *Hausmann and Platt*, 1994; *Tuckermann et al.*, 1997].

[5] The coactivation of bromine and chlorine chemistry predicted by photochemical models [e.g., *Sander et al.*, 1997; *Michalowski et al.*, 2000] has been shown by direct measurements [*Jobson et al.*, 1994; *Tuckermann et al.*, 1997]. Hydrocarbons are particularly useful proxies. Light alkanes are oxidized by Cl radicals and acetylene is oxidized by both Br and Cl radicals. The temporal mean concentrations of halogen radicals can therefore be estimated by investigating the losses of light alkanes and acetylene [*Jobson et al.*, 1994; *Solberg et al.*, 1996; *Ariya et al.*, 1998; *Ramacher et al.*, 1999; *Boudries and Bottenheim*, 2000].

[6] Satellite measurements of BrO by the Global Ozone Monitoring Experiment (GOME) represent a major advancement in our capability to monitor halogen radicals in the Arctic spring [*Richter et al.*, 1998; *Chance*, 1998; *Wagner and Platt*, 1998]. The spatial and temporal coverage of GOME far exceeds the available surface aircraft measurements of any chemical species related to halogen chemistry. Taking advantage of this new capability, *Zeng et al.* [2003] prescribed BrO concentration on the basis of GOME measurements in March and April 2000 in a regional chemical transport model (RCTM) to evaluate the model simulated low-altitude ozone losses driven by bromine chemistry with surface and aircraft observations and to investigate the spatial and temporal extents of near-surface ozone depletions, which cannot be determined from available in situ or remote sensing observations.

[7] The Tropospheric Ozone Production about the Spring Equinox (TOPSE) experiment took place from February to May in 2000. Measurements of ozone, reactive nitrogen, and hydrocarbons are made from 40 to 85°N and from the surface up to 8 km. In this work, we extend the model study of *Zeng et al.* [2003] to the entire period of TOPSE observations. We systematically evaluate simulated ozone concentrations with the observations from TOPSE and two surface sites. Furthermore, light alkanes and acetylene are simulated to investigate the additional observational constraints by aircraft measurements of these halogen proxies. We also investigate the sensitivities of halogen-induced ozone and hydrocarbon losses to the key model parameter, the boundary layer height of halogen chemistry. We describe the model setup and data processing in section 2. Simulations and evaluations of low-altitude ozone are discussed in section 3. The simulations of light alkanes and acetylene measurements are presented in section 4. Conclusions are given in section 5.

2. Methodology

2.1. Model Description

[8] The regional three-dimensional chemical transport model has been previously used by *Zeng et al.* [2003] and *Choi et al.* [2005]. The polar version of the Penn State/National Center for Atmospheric Research (NCAR) mesoscale model MM5 [*Bromwich et al.*, 2001; *Cassano et al.*, 2001] is used to generate the meteorological fields using four-dimensional data assimilation with the National Center for Environmental Prediction (NCEP) reanalysis, surface, and rawinsonde observations. Polar MM5 has cloud physics and radiative transfer parameterizations more suitable for polar regions. A series of 6-day polar MM5 assimilations are conducted and the last 5-day data assimilation products are combined to produce 4-month meteorological fields to drive the RCTM. The model domain has 106×106 grids centered at the North Pole with a horizontal resolution of 80 km (Figure 1). There are 22 vertical layers extending up to 10 hpa, eight of which are located in the lowest 1 km to better simulate the shallow boundary layer at high latitudes. The tops of the lowest eight layers are 16, 40, 80, 200, 320, 480, 650, and 1000 m, respectively.

[9] Relative to halogen chemistry, the lifetimes of ozone and nonmethane hydrocarbons (NMHCs) due to losses through tropospheric O_3-NO_x-HO_x chemistry are much longer. As a result, chemical boundary conditions for these chemicals are often more important than chemical reactions inside the regional model domain. We make use of the global GOES-CHEM simulation results with ''normal'' tropospheric chemistry in our RCTM and focus our attention on halogen-related chemistry.

[10] GEOS-CHEM [*Bey et al.*, 2001] simulations are used to prescribe model initial and chemical boundary conditions. We employ GEOS-CHEM version 5.02 (a horizontal resolution of $4° \times 5°$ with 48 layers up to 0.01 hpa) driven by assimilated meteorological fields (GEOS-3) from the Goddard Earth Observing System (GEOS) of the NASA Global Modeling Assimilation Office (GMAO). We set the upper chemical boundary condition at 3 km for RCTM since our concern is in the lower troposphere. For ozone simulations, we archive hourly GOES-CHEM ozone production rates and loss frequencies and use them in the RCTM in combination with our estimation of bromine driven losses. For NMHC simulations, we use hourly archived OH fields from GEOS-CHEM. The changes of OH at low altitudes due to halogen chemistry are assumed to be insignificant [*Evans et al.*, 2003].

[11] We use NMHCs as proxies to estimate the concentrations of Cl and Br radicals [*Jobson et al.*, 1994]. There is in general a strong association between the activations of Br and Cl radicals [*Vogt et al.*, 1996; *Foster et al.*, 2001], and both tend to have high concentrations when ozone depletion occurs [*Jobson et al.*, 1994; *Tuckermann et al.*, 1997]. Differential reaction rates of NMHCs with halogen radicals leave fingerprints for Cl and Br concentrations over their loss by OH oxidations [e.g., *Jobson et al.*, 1994; *Ramacher et al.*, 1999]. Light alkanes are oxidized significantly by Cl,

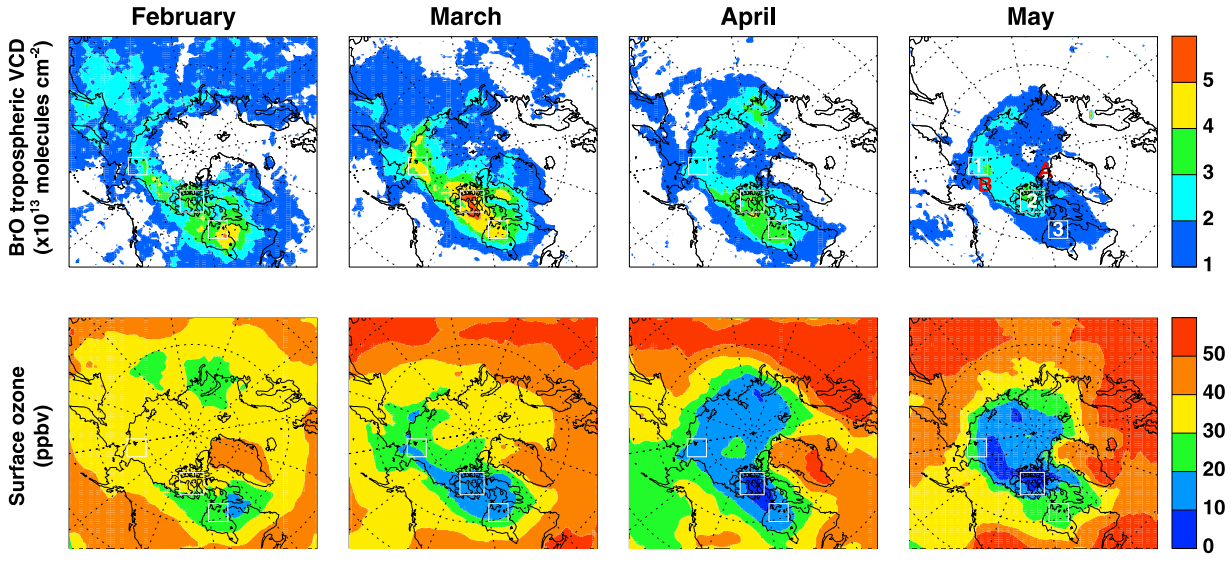

Figure 1. GOME BrO tropospheric vertical columns and simulated near-surface O_3 concentrations over the model domain from February to May 2000. The locations of the two surface sites, Alert, Canada (82.5°N, 62.3°W) (marked by "A"), and Barrow, Alaska (71.3°N, 156.6°W) ("B"), are shown in the fourth panel of the top row. Three regions with BrO column $>4 \times 10^{13}$ molecules cm^{-2} are shown by white squares over the Chukchi Sea, Canadian archipelago, and northern Hudson Bay.

while acetylene is oxidized substantially by Cl and Br. Benzene does not react significantly with either Cl or Br.

[12] GEOS-CHEM simulates explicitly O_3, C_2H_6, and C_3H_8 but not C_2H_2, C_6H_6, i-C_4H_{10}, or n-C_4H_{10}. However, Table 1 shows the good correlations between observed hydrocarbon tracers during the TOPSE experiment. In order to specify the proper chemical boundary conditions for the RCTM simulations, we make use of the observed linear relationships (Table 1) to scale the boundary values of C_2H_2 and C_6H_6 to GEOS-CHEM simulated C_3H_8. GEOS-CHEM simulates a lumped ALK4 tracer for $\geq C_4$ alkanes. We use the observed i-C_4H_{10} and n-C_4H_{10} fractions to ALK4 (Table 1) to specify their boundary conditions.

[13] Initial evaluation of GEOS-CHEM simulations of NMHCs revealed a general underestimation by the model. Given their relatively long lifetime, the low biases in the boundary values of these tracers will result in low biases in the RCTM simulations. To correct for the biases, we binned TOPSE and GEOS-CHEM data into monthly averages per 5° latitudes and 1-km altitude. The observed to simulated ratios are applied to scale the GEOS-CHEM-derived chemical initial and boundary conditions. The scaling factors are in the range of 0.5 to 2. The scaling is reasonable for the polar region because the meteorological conditions in the region tend to be homogeneous and there are no significant pollutant sources [*Gautrois et al.*, 2003]. A similar scaling was applied to the initial and boundary conditions of ozone even though the model bias is much less than those of NMHCs when compared to TOPSE observations. The emissions of NMHCs in the RCTM are adopted from *Piccot et al.* [1992] as modified by *Wang et al.* [1998]. The molar emission ratios of C_2H_2 and C_6H_6 to C_2H_6 are 0.933 and 0.467, respectively, and those of i-C_4H_{10}, and n-C_4H_{10} to ALK4 are 0.190 and 0.775, respectively [*Middleton et al.*, 1990].

[14] We do not explicitly simulate the halogen chemistry in the RCTM in part because our understanding of halogen sources is too limited at present to simulate in 3-D models [e.g., *Michalowski et al.*, 2000]. We instead use the GOME observations of BrO (next section) to prescribe halogen radical distributions in the RCTM and evaluate the constraints on these distributions by the observations of proxy species like ozone and NMHCs. We scale daytime (solar zenith angle < 89°) Br concentrations to BrO [*Platt and Janssen*, 1995],

$$\frac{[\mathrm{BrO}]}{[\mathrm{Br}]} = \frac{k_{\mathrm{Br+O_3}}[\mathrm{O_3}]}{2k_{\mathrm{BrO+BrO}}[\mathrm{BrO}] + k_{\mathrm{BrO+ClO}}[\mathrm{ClO}] + k_{\mathrm{BrO+NO}}[\mathrm{NO}] + J_{\mathrm{BrO}}} \quad (2)$$

Table 1. Correlations Coefficients[a] Between NMHCs Observed During TOPSE

Species, pptv	Linear Fitting Equation	r^2	Standard Deviation, pptv
C_2H_2 versus C_3H_8	$[C_2H_2] = 0.443[C_3H_8] + 182.773$	0.835	80.2
C_6H_6 versus C_3H_8	$[C_6H_6] = 0.126[C_3H_8] + 25.117$	0.850	21.4
n-C_4H_{10} versus ALK4[b]	$[n\text{-}C_4H_{10}] = 0.477[ALK4] + 10.305$	0.997	8.0
i-C_4H_{10} versus ALK4[b]	$[i\text{-}C_4H_{10}] = 0.243[ALK4] + 7.763$	0.994	5.7

[a]For conditions without significant influence by halogen chemistry ($[O_3] \geq 20$ ppbv).
[b]ALK4 includes n-C_4H_{10}, i-C_4H_{10}, n-C_5H_{12}, i-C_5H_{12}, C_6H_{14}.

The BrO_x cycling by the reactions of BrO and HO_2 followed by photolysis of HOBr is not considered because the relative small effect compared to reactions considered in equation (2) and a lack of HO_2 measurements. We calculate NO concentrations on the basis of the observed correlation between NO and ozone during TOPSE [*Evans et al.*, 2003]. The concentration of ClO is assumed to be equal to the concentration of BrO [*Tuckermann et al.*, 1997]. Using a smaller ClO/BrO ratio in the calculation does not change the model results. We further assume that daytime BrO_x (dominated by BrO) does not vary [*Evans et al.*, 2003].

[15] The Br/BrO partition depends mainly on the concentrations of ozone and the photolysis rate of BrO (J_{BrO}). The latter accounts for >90% of the conversion from BrO to Br. We calculate the J_{BrO} values using the four-stream NCAR Tropospheric Ultraviolet-Visible (TUV) radiation model (version 4.2) [*Madronich and Flocke*, 1998]. There are three key parameters in the calculation: solar zenith angle, ozone column, and cloud optical depth. The latter two are obtained from the Total Ozone Mapping Spectrometer (TOMS) and GOME, respectively.

[16] The evaluation of our ozone simulations with TOPSE measurements depends on the prescribed BrO levels (equation (1)). We estimated the ozone loss due to the ClO-BrO reaction by comparing the reaction rate of Cl + O_3 to that of BrO + BrO. The fraction of ClO that reacts with NO leading to a null cycle is not considered. Using our best estimates of Cl concentrations (to be described in section 4.3) and observed NO as a function of ozone during TOPSE, we found that the O_3 loss due to ClO is about 10% of that driven by BrO-BrO and Br-O_3 reactions. It is therefore not included in the O_3 loss calculation. Additional ozone loss through the reaction of BrO and HO_2 is not included either.

2.2. GOME BrO Measurements

[17] GOME measures nadir-viewing backscattered radiances over the spectral range 240–800 nm with a spatial resolution of 320 × 40 km^2 [*European Space Agency*, 1995]. Analyses of GOME spectra previously showed high BrO concentrations at northern and southern high latitudes in spring [*Richter et al.*, 1998; *Chance*, 1998; *Wagner and Platt*, 1998]. We obtain the BrO slant column density (SCD) through direct fitting to the radiance measurements [*Chance*, 1998]. Stratospheric and tropospheric air mass factors (AMFs) [*Chance*, 1998] are applied to convert the SCD to vertical column density (VCD = SCD/AMF). The tropospheric AMF was calculated for a thickness of 500 m and an average surface UV albedo of 0.8. GOME-observed cloud fractions were used in the calculation [*Martin et al.*, 2002]. Three-day BrO averages are necessary for the full model domain coverage. In case of missing and highly biased data (in late March), 5-day averages are used. Taking advantage of the homogeneity of stratospheric BrO (compared to the troposphere), we obtain the daily stratospheric column by taking the 10th percentile column for each half-degree latitude band. Such determined stratospheric columns are consistent with previous estimates [*Fitzenberger et al.*, 2000; *Wagner et al.*, 2001]. The tropospheric column is then computed by subtracting the stratospheric VCD from the total VCD and readjusting for the reduced tropospheric AMFs.

[18] The vertical distribution of BrO concentrations in the polar lower troposphere is uncertain. High-BrO and low-ozone events are usually associated with strong inversion, which reduces vertical mixing [*Gong et al.*, 1997]. Observed ozone depletion depths range from several hundred meters to above 1 km depending on the meteorological conditions [*Tarasick and Bottenheim*, 2002]. Various thicknesses have been used in model studies including 200 m [*Evans et al.*, 2003], 400 m [*Zeng et al.*, 2003], and 600 m [*Sumner and Shepson*, 1999]. We find that ozone concentrations are very sensitive to the BrO layer thickness because of the quadratic dependence of ozone loss on BrO concentrations. In this work, we conduct 5 sensitive simulations with the BrO layer thickness of 100, 200, 300, 400, and 1000 m. We find that a thickness of 300 m gives the best comparison of model results with surface ozone observations at Alert and Barrow and aircraft ozone vertical profiles measured during TOPSE. The tropospheric AMF values are insensitive to a BrO layer thickness ranging from 200 to 500 m.

[19] On the basis of aircraft measurements of BrO column on 16 April 1997, *McElroy et al.* [1999] suggested that free tropospheric BrO could significantly contribute to the total tropospheric BrO column. One key constraint in the analysis is that boundary layer BrO mixing ratio is <50 pptv. The observed BrO VCD in that study is (1–3) × 10^{14} molecules cm^{-2}. In our analysis, out of > 280,000 BrO VCDs from GOME in April 2000, there are only 7 VCDs > 1 × 10^{14} molecules cm^{-2}. Furthermore, Figure 1 illustrates that the high-BrO regions are inaccessible for ground based in situ measurements. The fact that previous measurements generally showed boundary layer BrO mixing ratios of <50 pptv does not imply that the BrO mixing ratios cannot be >50 pptv over those high-BrO regions. Given the lack of critical measurements that can quantitatively constrain free tropospheric BrO, we assume that free tropospheric BrO column is negligible in this study.

3. Ozone

3.1. Seasonal Transition of Near-Surface Ozone Concentrations

[20] Figure 1 shows monthly mean tropospheric BrO columns and the corresponding model simulated surface ozone concentrations from February to May in 2000. Overall low-ozone regions collocate with high-BrO regions. The maximum BrO column appears in March whereas the area of near-surface ODEs (O_3 < 20 ppbv) peaks in April. The time delay reflects longer daytime hours that allow for chemical processing. By May, high bromine column areas retreat back to higher latitudes over the Arctic Ocean. The magnitude and coverage of simulated ozone depletion decrease as a consequence.

[21] In order to examine the potential factors related to bromine activation, we identify in Figure 1 three regions with high tropospheric BrO column [*Zeng et al.*, 2003]. We extend the correlation analysis to a longer period from February to May; Region 1 is enlarged to include the entire Chukchi Sea in order to include high BrO observed in May over this region. Among the various meteorological factors including temperature, pressure, wind speed, and relative humidity, temperature has the highest (anti)correlation with

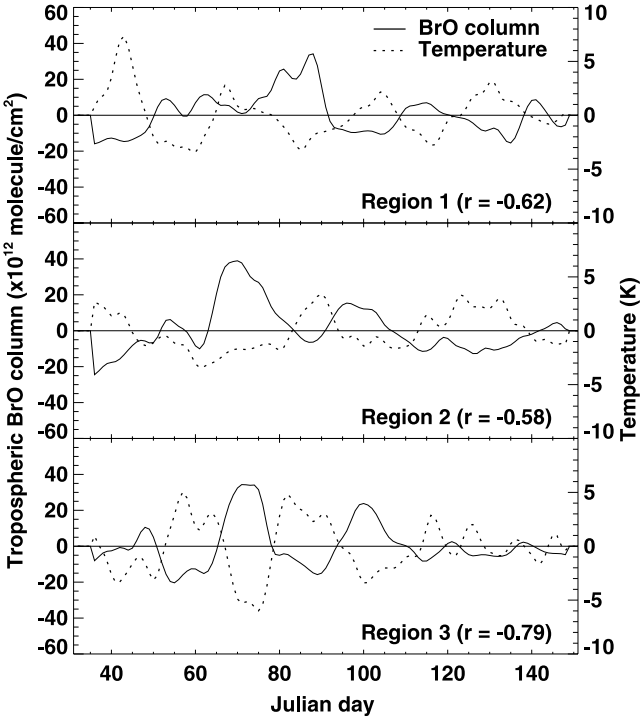

Figure 2. Daily GOME BrO tropospheric vertical columns (10^{14} molecules/cm^2) and model assimilated surface temperature (K) over the three regions defined in Figure 1. The linear seasonal trends of BrO column and temperature are removed. Also shown are the correlation coefficients between the two parameters.

tropospheric BrO column. Figure 2 shows the correlations between daily mean tropospheric BrO columns and assimilated surface temperatures for the three regions after their linear trends are removed. The correlation coefficients during the 4 months are −0.62, −0.58, and −0.79 respectively. Large negative temperature anomalies correspond to large positive BrO anomalies. For instance, the largest BrO enhancements at three regions on Julian days 88, 70, and 75 occurred at the same time as the largest temperature deviations of −3.2, −3.3, and −6.3 K respectively. In May, BrO column varies less when temperature has smaller fluctuations.

[22] This negative correlation is consistent with bromine activation in sea-salt aerosols in the atmosphere or deposited on ice/snow [*Barrie et al.*, 1988; *Tang and McConnell*, 1996]. *Koop et al.* [2000] found that the surface of sea-salt aerosols remained in quasi-liquid phase at temperature down to 230 K and that the Br^- concentrations in aerosols increase by more than an order of magnitude as temperature decreases. The presence of small amount of chemicals like HOBr will result in rapid release of bromine through their reactions with Br^- [e.g., *Fan and Jacob*, 1992]. Frost flower formation at lower temperature may also contribute to the activation of Br radicals [*Rankin et al.*, 2002; *Kaleschke et al.*, 2004]. The temporal variations of surface temperature in regions 2 and 3 are generally in phase, while they are out of phase from that in region 1. The spatial correlation of regional surface temperature reflects the movement of cold polar air masses.

3.2. Ozone at Alert and Barrow

[23] We compare in Figure 3 the simulated near-surface ozone concentrations with the measurements at Alert, Canada (82.5°N, 62.3°W) (K. Anlauf, personal communication, 2002) and Barrow, Alaska (71.3°N, 156.6°W) [*Oltmans and Levy*, 1994]. The correlation coefficients are 0.59 and 0.67 for Alert and Barrow, respectively. The model-measurement correlations at Barrow and Alert are better than those simulated for March and April by *Zeng et al.* [2003]. The ETA Mellor-Yamada-Janjic 2.5-order closure scheme in MM5 assumed a minimum for diffusion coefficient at

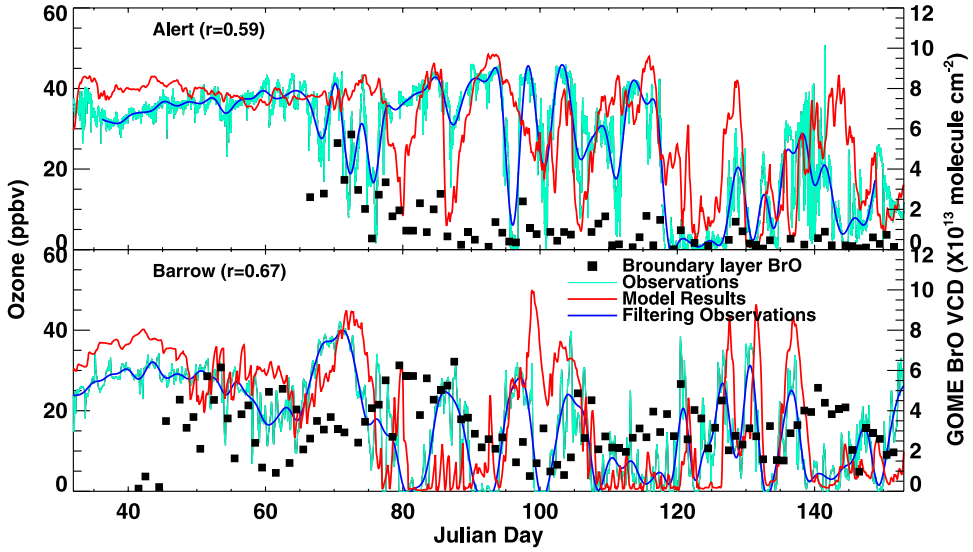

Figure 3. Tropospheric GOME BrO vertical columns and observed and simulated O_3 concentrations at Alert, Canada, and Barrow, Alaska, from February to May 2000. Three-day low-pass filtered O_3 observations are also shown. The frequency of O_3 measurement at Alert is every 5 min; it is hourly at Barrow. The correlation coefficients are calculated using 4-hour averages.

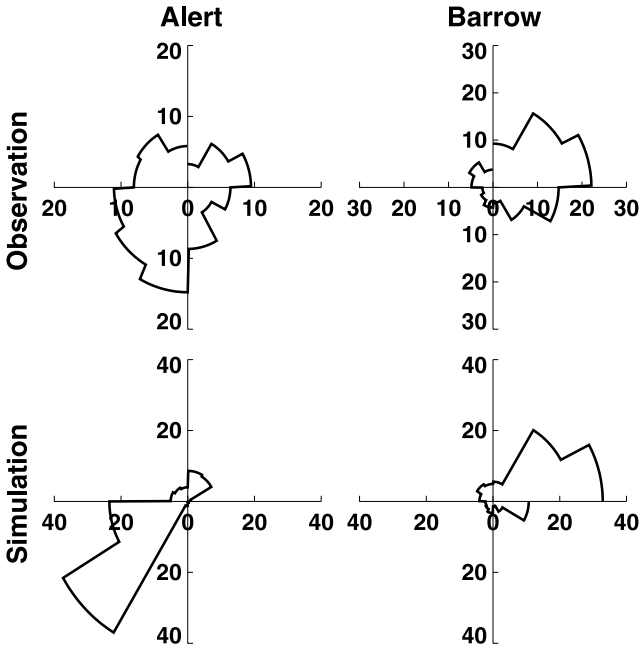

Figure 4. Observed and simulated percentage frequencies of wind directions at Alert, Canada, and Barrow, Alaska. The wind direction interval is 30°.

0.09 m^2 s^{-1}, which was used in our previous study. By reducing the minimum to 10^{-3} m^2 s^{-1}, we find that simulated surface ozone concentrations at Alert are in better agreement with the observations; the improvement is particularly large in May. Furthermore, ongoing investigations indicate that the lower diffusion coefficient minimum is essential in order to reproduce the observed boundary layer height by sonic detection and ranging (SODAR) over the South Pole (Y. Wang et al., Assessing the photochemical impact of snow NO_x emissions over Antarctica during ANTCI 2003, submitted to *Atmospheric Environment*, 2006). The surface roughness of snow/ice surface is much lower than common land types at mid latitudes. The default diffusion coefficient minimum is more appropriate for the latter.

[24] The ozone simulation at Barrow is better than Alert (Figure 4) since the polar MM5 assimilated wind fields are more consistent with the observations at Barrow [e.g., *Oltmans and Levy*, 1994; D. Worthy, personal communication, 2004]. Our model with a horizontal resolution of 80x80 km^2 cannot capture the complexity of surrounding topography at Alert, which contributes to errors in the simulation results. Assimilated surface winds at Barrow are mostly northeasterlies similar to the observations. Assimilated surface winds at Alert are mostly from the southwest in contrast to the broadly distributed wind directions in the observations, although the southwest portion of the observed wind directions is the largest.

[25] The ozone simulations at Alert are also more sensitive to transport. Figure 3 shows higher-BrO columns at Barrow than Alert. There is no anticorrelation between observed surface ozone and BrO columns at Barrow (r = −0.15). In comparison, the BrO columns at Alert even show a weak positive correlation with ozone observations (r = 0.33), further indicating the insignificance of in situ ozone loss. Long-range transport of ozone-poor air largely regulates the low-ozone events at Alert and contributes significantly to low ozone at Barrow. Winds at Barrow mostly vary from east to northeast in this period (Figure 4). Wind directions are more random at Alert. Generally, Alert is affected more by transport from the southwest and less from the southeast. Regions 2 and 3 with high-BrO columns and low ozone concentrations (Figure 1) are likely the source regions of low-ozone air observed at these sites.

[26] We apply a back trajectory model using polar MM5 assimilated wind fields [*Zeng*, 2005] to investigate the impact of long-range transport. Back trajectories show that these two sites are strongly affected by air masses transported from Canadian Archipelago (region 2). Air masses transported from region 3 also affect Barrow. No air mass is transported from region 1 to the two sites.

[27] The ozone depletion events observed at Barrow clearly show three cycles with a 10-day period from Julian day 80 to 110 and four cycles with a 5-day period from Julian day 120 to 140. Although not as clear as shown at Barrow, ozone depletion at Alert shows four cycles with a 7-day period from Julian day 96 to 118. These changes occur at higher frequencies than those of regional high-BrO columns shown in Figure 2. The periodicity could be driven by oscillations in small-scale meteorological systems that affect transport of ozone-poor air from high-BrO regions to these two sites. More work on the circulation changes in the region is necessary before we can fully understand the observed periodicities.

3.3. Vertical Ozone Profiles

[28] We bin TOPSE in situ ozone measurements into three latitude bands, middle (50–60°N), mid-high (60–70°N), and high (>70°N). Figure 5 compares the observed monthly mean ozone profiles with corresponding model simulations from March to May up to the upper chemical boundary at 3 km. A sensitivity simulation without BrO-driven loss is also shown. February comparison is not included because there is no evidence of significant halogen impact on ozone. During the 3-month period, ozone mixing ratios at the upper boundary (3 km) increase by 5–10 ppbv driven largely by tropospheric NO_x chemistry [*Browell et al.*, 2003; *Wang et al.*, 2003a]. The standard model simulations are generally within the observed standard deviations with few exceptions. The large underestimation of low-altitude ozone at 60–70°N in March will be discussed in detail in section 4.2.

[29] At the lowest 1 km, the observations show a clear decreasing ozone trend toward the surface. The model reproduces this vertical gradient and the altitude at which the apparent ozone loss occurs. By comparing the standard and sensitivity simulations, it is clear that the vertical gradient is mainly due to BrO catalyzed ozone loss. The largest effects of halogen chemistry on ozone are in April consistent with the distributions seen in Figure 1. The reduction of ozone from 1 km to the surface reaches 40 ppbv at 60–70°N in that month. The model has a tendency to overestimate ozone concentrations at high latitudes (north of

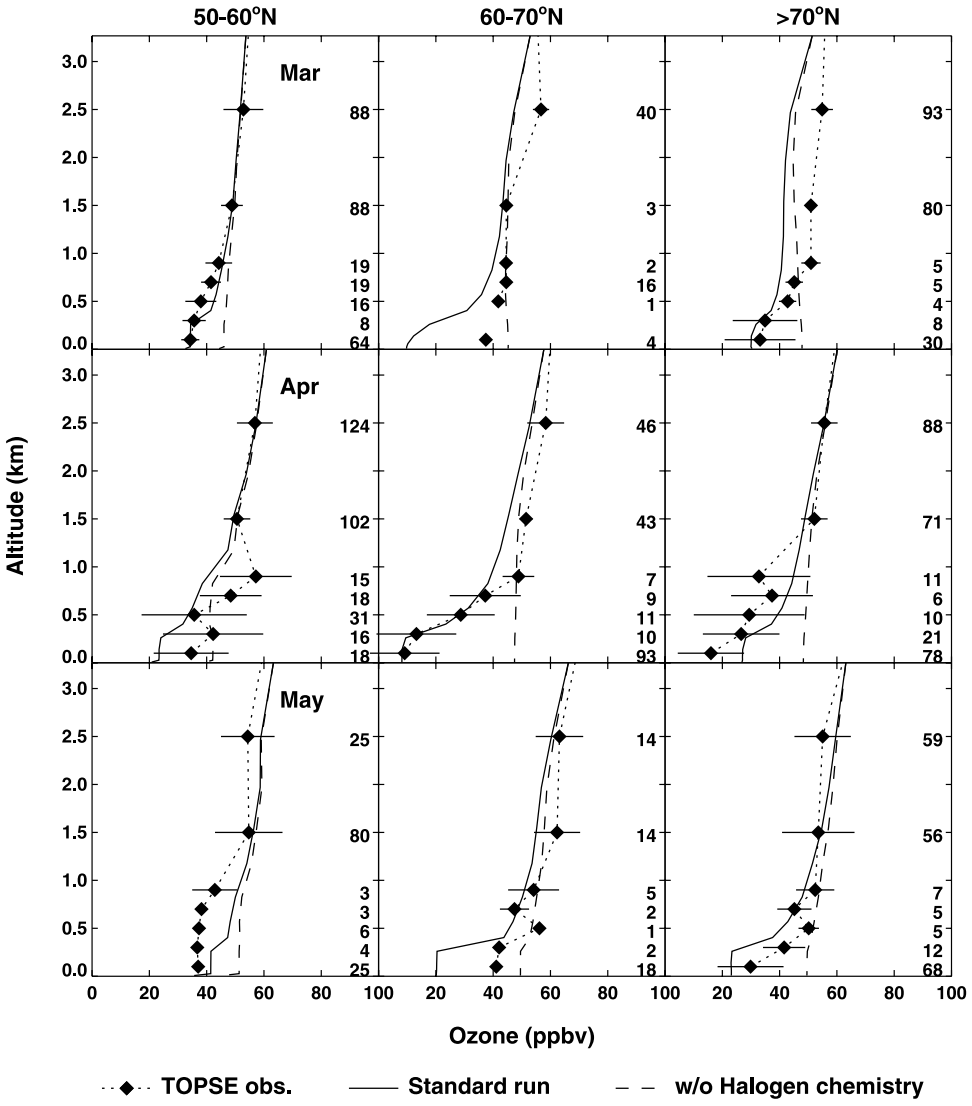

Figure 5. Observed and simulated monthly mean ozone profiles at three latitudinal bands, 50–60°N, 60–70°N, and >70°N. Model results are shown with and without bromine chemistry. Model data are selected corresponding to the time and location of measurements. The horizontal bar shows the observed standard deviation. Number of measurement samples in each model layer is also shown.

70°N), which likely reflects in part the larger uncertainties in GOME retrievals at higher solar zenith angles.

4. NMHCs

4.1. Empirical and Theoretical Br/Cl Functions

[30] Direct measurements [*Tuckermann et al.*, 1997] and indirect evidence [*Jobson et al.*, 1994; *Solberg et al.*, 1996] show simultaneous Cl and Br increases during polar spring. In our model simulations, we calculate Br on the basis of GOME-derived BrO concentrations (equation (2)). The calculated Br/BrO ratios are largely functions of ozone and the photolysis rate of BrO (section 2.1), both of which are reasonably well known. There are two methods of calculating Cl/Br ratios. The box model by *Evans et al.* [2003] incorporated a heterogeneous halogen chemical mechanism [*Michalowski et al.*, 2000] and calculated the concentrations of Cl and Br as a function of ozone.

[31] The second possibility is to use the empirical relationships derived by *Ramacher et al.* [1999] on the basis of the observations of NMHCs during ODEs. They calculated integrated Cl and Br concentrations using equations (3) and (4),

$$-\int_{t_0}^{t_x}[\mathrm{Cl}]dt = \frac{1}{k_{\mathrm{alkane,Cl}}}\ln\left(\frac{[\mathrm{alkane}]_x}{[\mathrm{alkane}]_0}\right) \tag{3}$$

$$-\int_{t_0}^{t_x}[\mathrm{Br}]dt = \frac{1}{k_{\mathrm{C_2H_2,Br}}}\left(\ln\left(\frac{[\mathrm{C_2H_2}]_x}{[\mathrm{C_2H_2}]_0}\right) + k_{\mathrm{C_2H_2,Cl}}\int_{t_0}^{t_x}[\mathrm{Cl}]dt\right) \tag{4}$$

They fitted the derived Cl and Br integrals as a function of ozone and obtained the following empirical relationships [*Ramacher et al.*, 1999],

Table 2. Kinetics Data of the Reactions

	Reactions	Reaction Rate Constant	References
(5)	OH + C_2H_6	8.7×10^{-12} exp(−1070/T)	*Sander et al.* [2003]
(6)	OH + C_3H_8	1.0×10^{-11} exp(−660/T)	*Sander et al.* [2003]
(7)	OH + C_6H_6	$9.3 \times 10^{-12}(T/298)^{-1.18}$ exp(−5138/RT)	*Lay et al.* [1996]
(8)	OH + C_2H_2	$k_0 = 5.5 \times 10^{-30}$, $k_\infty = 8.3 \times 10^{-13}$ $(T/300)^2$ $k(M, T) = \left(\frac{k_0[M]}{1+k_0[M]/k_\infty}\right)0.6^{\left\{1+[\log_{10}(k_0[M]/k_\infty)]^2\right\}^{-1}}$	*Sander et al.* [2003]
(9)	OH + i-C_4H_{10}	1.5×10^{-12} $(T/298)^2$ exp(145/T)	*Warneck* [1999]
(10)	OH + n-C_4H_{10}	1.0×10^{-12} $(T/298)^2$ exp(235/T)	*Warneck* [1999]
(11)	Cl + C_2H_6	7.7×10^{-11} exp(−90/T)	*Sander et al.* [2003]
(12)	Cl + C_3H_8	1.2×10^{-10} exp(−40/T)	*Sander et al.* [2003]
(13)	Cl + C_2H_2	$k_0 = 5.9 \times 10^{-30}$ $(T/300)^{-2.1}$, $k_\infty = 2.1 \times 10^{-10}$ $(T/300)^{-1}$ $k(M, T) = \left(\frac{k_0[M]}{1+k_0[M]/k_\infty}\right)0.6^{\left\{1+[\log_{10}(k_0[M]/k_\infty)]^2\right\}^{-1}}$	*Sander et al.* [2003]
(14)	Cl + n-C_4H_{10}	1.7×10^{-10} exp(56/T)	*Atkinson and Aschmann* [1985]
(15)	Cl + i-C_4H_{10}	1.37×10^{-10}	*Atkinson and Aschmann* [1985]
(16)	Br + C_2H_2	6.35×10^{-15} exp(440/T)	*Atkinson et al.* [2002]
(17)	Br + O_3	1.7×10^{-11} exp(−800/T)	*Sander et al.* [2003]
(18)	BrO + BrO	1.5×10^{-12} exp(−230/T)	*Sander et al.* [2003]

$$\int [\mathrm{Cl}]dt/10^9 = -0.2256\chi_{O_3} + 9.2813 \tag{5}$$

$$\int [\mathrm{Br}]dt/10^9 = -2.3122\ln\chi_{O_3} + 8.5697 \tag{6}$$

where [Cl] and [Br] are in the unit of molecules cm^{-3} and χ_{O_3} is the mixing ratio of ozone in the unit of ppbv.

[32] To make use of the empirical results and compare to the theoretical calculation by *Evans et al.* [2003], we transform the Br and Cl integrals into Br/Cl ratios as function of ozone. The ozone depletion rate by BrO (equation (1)) can be rewritten as

$$\frac{d[\mathrm{O_3}]}{dt} = -2k_{\mathrm{BrO+BrO}}[\mathrm{BrO}]^2 \tag{7}$$

Using the above equation, we switch the integration variable from time (t) to [O_3] in equations (5) and (6) and obtain,

$$\int \frac{[\mathrm{Cl}]}{-2k_{\mathrm{BrO+BrO}}[\mathrm{BrO}]^2 \times 10^9/\rho_{air}} d[\mathrm{O_3}] = -0.2256\chi_{O_3} + 9.2813 \tag{8}$$

$$\int \frac{[\mathrm{Br}]}{-2k_{\mathrm{BrO+BrO}}[\mathrm{BrO}]^2 \times 10^{12}/\rho_{air}} d[\mathrm{O_3}] = -2.3122\ln\chi_{O_3} + 8.5697 \tag{9}$$

where ρ_{air} is air number density in the unit of molecules cm^{-3}. After differentiation with respect to [O_3], we obtain the ratio of Br/Cl assuming simultaneous Br and Cl chemical processing,

$$\frac{[Br]}{[Cl]} = \frac{10250}{\chi_{O_3}} \tag{10}$$

Comparing equation (10) with the theoretical calculation by *Evans et al.* [2003], we find that the two results differ drastically particularly when ozone is <10 ppbv.

[33] To further evaluate the difference between the theoretical and empirical functions of Br/Cl ratio, we consider a simple box model for the oxidation of C_2H_6, C_3H_8, and C_2H_2 by OH, Cl, and Br and ozone loss due to Br chemistry (reactions (R5), (R6), (R8), (R11), (R12), (R13), (R16), (R17), and (R18) in Table 2). The model is initiated with 2 ppbv ethane, 1 ppbv propane, 500 pptv acetylene, 1×10^9 molecules cm^{-3} BrO, 1×10^6 molecules cm^{-3} OH, and 40 ppbv O_3. To further simplify the interpretation of the calculation results, we hold OH and BrO concentrations constant. The concentration of Br is calculated as in the regional CTM (equation (2)). The Cl/Br ratio is calculated using either the empirical relationship by *Ramacher et al.* [1999] (equation (10)) or the theoretical one by *Evans et al.* [2003]. The model generated time evolutions of NMHCs and O_3 are archived and we diagnose the integrated Br and Cl concentrations in the same manner as *Ramacher et al.* [1999].

[34] Figure 6 shows the resulting ratio of time integrated Br and Cl as a function of ozone for a typical polar sunrise condition. The curve calculated using equation (10) is essentially the same as that by *Ramacher et al.* [1999]. The slight deviation is due to our inclusion of OH oxidation; the result is consistent with the notion that halogen oxidation is much more dominant than OH. The time integrated Br/Cl ratios based on the theoretical calculation by *Evans et al.* [2003] also exhibit an exponential increase with decreasing ozone, but the ratios are about a factor of 2 less than those based on *Ramacher et al.* [1999]. Therefore we expect significantly different results when applying the empirical and theoretical Br/Cl relationships in the RCTM. We use TOPSE observations of NMHCs to evaluate these simulations and examine the implications on our current understanding of halogen chemistry.

4.2. Vertical Profiles of NMHCs

[35] We compare here the observed monthly mean vertical profiles of ethane, propane, and acetylene to model simulations from March to May at three latitude bands.

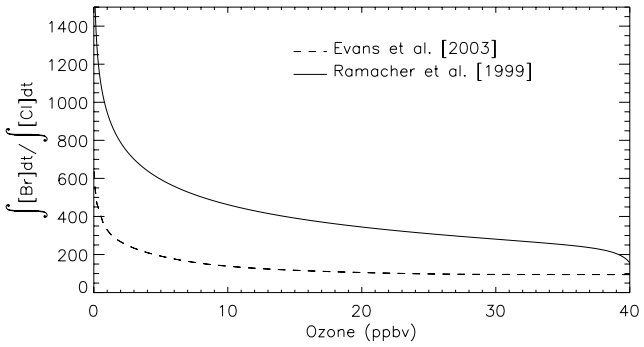

Figure 6. Ratios of time integrals of Br and Cl concentrations for a typical polar sunrise condition (T = 250 K, solar zenith angle = 80°) using equation (10) derived from the empirical relationship of Br/Cl ratios by *Ramacher et al.* [1999] and the theoretical calculation by *Evans et al.* [2003].

Three model simulations are shown, without halogen oxidation, with the Br/Cl function calculated on the basis of *Ramacher et al.* [1999] (equation (10)), and with the Br/Cl function calculated by *Evans et al.* [2003]. Figures 7a and 7b show the comparisons for ethane and propane, respectively. NMHC concentrations decrease in spring because of increasing photochemical oxidation (mostly by OH) [*Blake et al.*, 2003; *Gautrois et al.*, 2003]. Box model [*Wang et al.*, 2003b] and our GEOS-CHEM simulations show one order of magnitude increase of monthly OH concentrations during the spring transition period. Rapid photochemistry is driven in part by increasing solar insolation and more abundant water vapor with higher temperature. Ethane concentrations at 3 km decrease by 20% from March to May; the corresponding decrease of propane is as large as 70% because of faster OH oxidation of propane. The decreasing trends are similar at the three latitude bands.

[36] The models underestimate ethane concentrations in March, and the simulated effects of Cl oxidation were seen in the observations only at north of 70°N although there are too few measurements at 60–70°N (Figure 7a). In April and May, the observations show a clear decreasing trend of ethane toward the surface in the lowest 1 km. Without halogen oxidation, the model cannot reproduce the observed gradient. The simulations using the empirical function by *Ramacher et al.* [1999] are in good agreement with the observations. In comparison, the model results based on the Br/Cl function by *Evans et al.* [2003] overestimate the Cl oxidation. The comparison with observed propane shows a similar agreement (Figure 7b). The absolute difference between the simulations using the empirical and theoretical Br/Cl functions is smaller in the comparison for ethane partly because of the rapid decrease of propane concentrations.

[37] Figure 7c shows the comparison for acetylene. Unlike ethane and propane, acetylene is effectively oxidized by Br atoms in addition to Cl and OH. The difference of the two model simulations using the empirical and theoretical Br/Cl functions reflects the portion of acetylene oxidized by Cl atoms because Br and OH concentrations are the same. At 250 K, the reaction rate constant of Cl with acetylene is ~480 times that of Br. However, the integrated Br concentrations are also two orders of magnitudes larger than Cl (Figure 6). Inspections of Figures 5 and 7 show indications that the depth of halogen layer is underestimated at north of 70°N in March and 60–70°N in April, while the simulations are reasonable in other months/regions.

4.3. NMHCs as Proxies of Halogen Radicals

[38] The monthly mean comparisons shown in Figure 7 are instructive. However, the halogen oxidation effects are masked because ODEs are averaged with measurements without apparent halogen influence. In this section, we investigate the NMHC observations during ODEs when O_3 mixing ratios are <20 ppbv. After conducting the analysis detailed below, the measurements from four specific flights are used to evaluate the corresponding model simulations.

[39] We apply the analysis method by *Jobson et al.* [1994]. For alkane oxidation by Cl atoms, we rewrite equation (3) as,

$$\ln\left(\frac{[\text{alkane}]_{\text{Low O}_3}}{[\text{alkane}]_{\text{Background}}}\right) = -k_{\text{alkane,Cl}}\int_{t_0}^{t_x}[\text{Cl}]dt \qquad (11)$$

When alkanes are processed by the same amounts of Cl atoms (integrated with time), we can plot $\ln\frac{[\text{alkane}]_{\text{Low O}_3}}{[\text{alkane}]_{\text{Background}}}$ with respect to the reaction rate constant and the slope reflect the integrated Cl level. The deviation of acetylene away from the linear relationship reflects the oxidation by Br,

$$\ln\left(\frac{[C_2H_2]_{\text{LowO}_3}}{[C_2H_2]_{\text{Background}}}\right) = -k_{C_2H_2,\text{Br}}\int_{t_0}^{t_x}[\text{Br}]dt - k_{C_2H_2,\text{Cl}}\int_{t_0}^{t_x}[\text{Cl}]dt \qquad (12)$$

Benzene is included with the alkanes and acetylene because it is virtually inert to halogen oxidation, the reaction rate constant of which is 4 to 5 orders of magnitude smaller than those of alkanes and acetylene [*Sokolov et al.*, 1998; *Bierbach et al.*, 1999]. We define the background concentrations as the averages for aircraft samples with ozone mixing ratios between 30 and 60 ppbv under 2 km for each flight. "Low O_3" values are calculated for sample with ozone mixing ratios <20 ppbv.

[40] Figure 8 shows the observed and simulated relationships between $\ln\frac{[\text{alkane}]_{\text{Low O}_3}}{[\text{alkane}]_{\text{Background}}}$ and reaction rate constant (K) for ethane, propane, n-butane, i-butane, benzene, and acetylene during the selected four flights. We calculate the least squares fit through alkanes and benzene. The resulting slope reflects the magnitude of time integrated Cl (equation (11)). The deviation of acetylene data from the least squares line reflects integrated Br (equation (12)). Previous studies [*Jobson et al.*, 1994; *Ariya et al.*, 1998; *Ramacher et al.*, 1999] used a constant temperature in the reaction rate constant calculation. We use instead the in situ temperature. Although the rate constants are not strongly temperature-dependent (Table 2), we find that using observed temperature improves the least squares fits. Aircraft measurements are more likely to encounter variable environments than at a surface site.

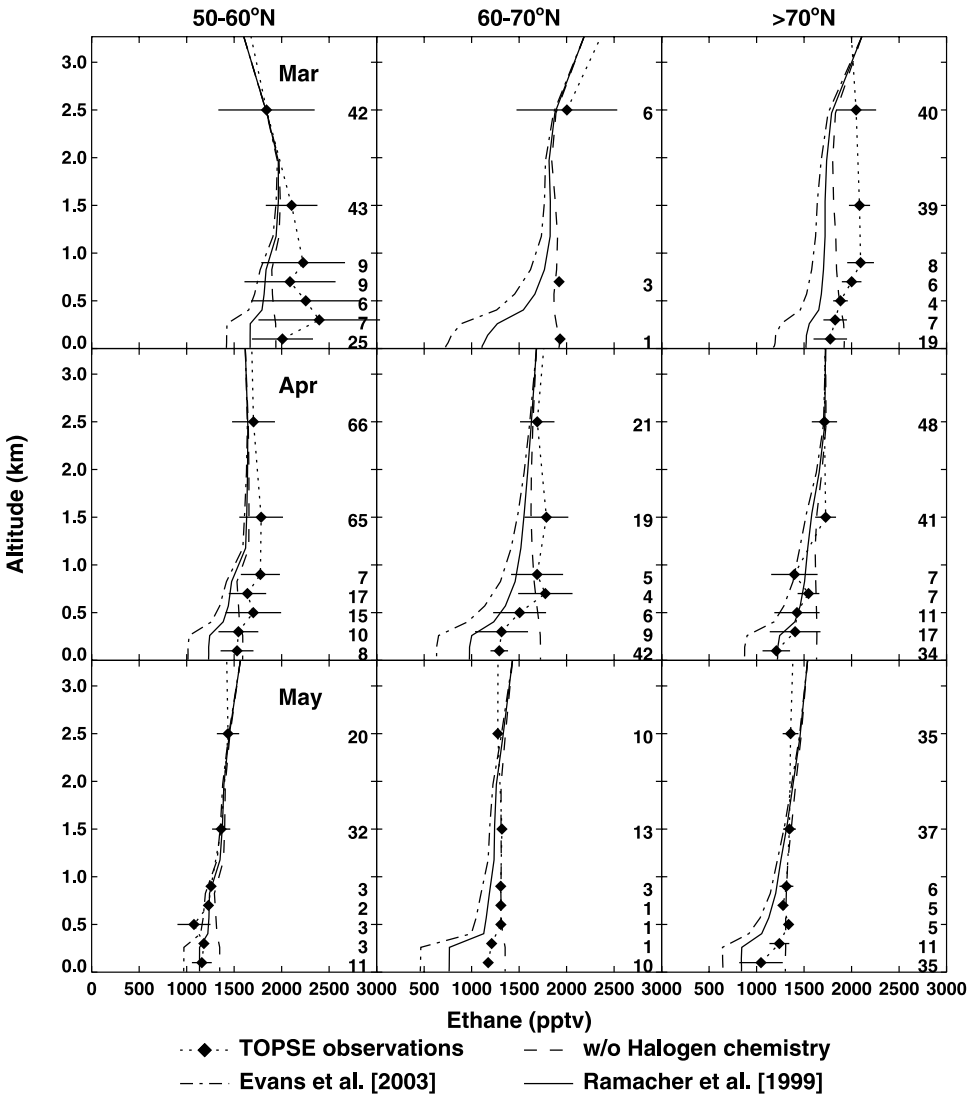

Figure 7a. Same as Figure 5 but for ethane. Three model simulations are shown, without halogen chemistry, using the empirical relationship of Br/Cl ratios by *Ramacher et al.* [1999] and using the theoretical calculation by *Evans et al.* [2003].

[41] We use these ODE cases to examine two specific questions. The first is whether these observations provide any constraints on the Br/Cl functions used in the model. The second is how sensitive the model results are to the specified thickness of the halogen layer. We therefore conduct the RCTM simulations using both the empirical Br/Cl function (equation (10)) derived from the work by *Ramacher et al.* [1999] and the box model calculation by *Evans et al.* [2003] for a thickness of 300 m. Two more sensitive simulations are conducted using the empirical Br/Cl function for the halogen layer depths of 200 and 400 m, respectively.

[42] Table 3 shows the slope values of the least squares fits in the observations and model simulations. Figure 8 compares the observations with model simulations with varying depths of the halogen layer using the empirical Br/Cl function by *Ramacher et al.* [1999]. Although Cl oxidation represented by the slopes match very well with the observations in 400-m BrO layer case, Br oxidation of C_2H_2 is underestimated for all four flights. With a halogen layer depth of 300 m in the standard simulations, BrO destruction of ozone and Cl oxidation of NMHCs are simulated well in the model. The absolute values of the simulated slopes have a bias of 2–35% using the empirical function derived from the work by *Ramacher et al.* [1999], suggesting that Cl atoms are overestimated. When using the box model calculation by *Evans et al.* [2003], the simulations generally lead to a higher degree of Cl oxidation, consistent with Figure 6. On two occasions (flights 26 and 34), the model overestimates by more than a factor of 2 the absolute values of the slopes in the measurements. The degree of overestimations differs from flight to flight likely reflecting the varying effects of turbulent mixing simulated by the 3-D model. Diagnosing the specific effects of mixing is complex and requires more dedicated studies [e.g., *Wang and Zeng*, 2004].

[43] Analyses of specific flights dominated by halogen oxidation discussed here and the evaluation of model

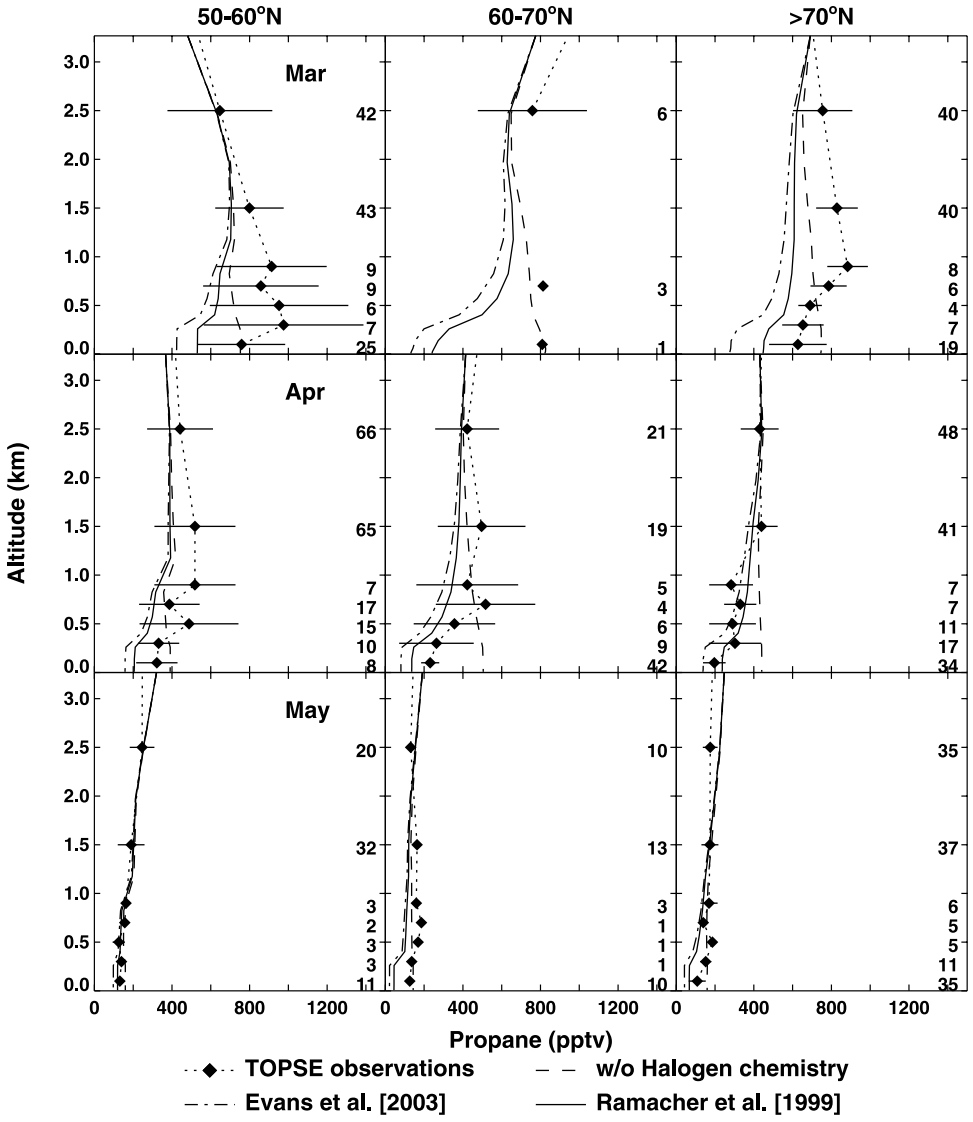

Figure 7b. Same as Figure 7a but for propane.

simulations with the observed profiles in the previous section suggest that the Cl/Br ratios during TOPSE are consistent with the measurements by *Ramacher et al.* [1999]. However, they are overestimated in the box model calculation by *Evans et al.* [2003], implying that the current halogen mechanism as used by *Evans et al.* [2003] and previous model studies overestimates the Cl/Br ratios. It is possible that the model overestimates the Cl^-/Br^- ratio in aerosols. However, total bromine is about half of total chlorine in the box model by *Evans et al.* [2003]. It is much higher than the 1:650 molar ratio of Br^-/Cl^- in seawater or 1:188 in the quasi-liquid surface of sea-salt aerosols at very low temperature [*Koop et al.*, 2000].

[44] The other possibility is that the box model overestimates Cl_2 concentrations. When ozone mixing ratio is >7 ppbv, gas-phase Cl_2 concentrations are estimated to be 3 times higher than BrCl by *Evans et al.* [2003]. On the other hand, the field studies by *Foster et al.* [2001] and *Spicer et al.* [2002] found Cl_2 was below the detection limit of 2 pptv; what they observed were high concentrations of BrCl with Br_2.

[45] Either the production of Cl_2 is overestimated or the loss is underestimated. In the currently accepted mechanism, Cl_2 is produced through the aqueous phase reaction $HOCl + Cl^- + H^+ \rightarrow Cl_2 + H_2O$. In the reactions, two kinetic parameters are highly uncertain, the reaction rate constant and Henry's Law constants of HOCl and Cl_2. The reaction rate constant (2.2×10^4 M^{-2} s^{-1}) was measured at 298 K [*Wang and Margerum*, 1994]. It decreases by a factor of 10 to 2.3×10^3 M^{-2} s^{-1} at 250 K on the basis of the thermodynamic calculation of Eyring Equation using the experiment results by *Wang and Margerum* [1994]. Large uncertainties are introduced in the model calculation because both the temperature dependence of the rate constant and temperature history of the air parcels are uncertain. The Henry's law constants were measured at bulk liquid conditions, which is very different from the quasi-liquid surface layer of snow and aerosols where the reactions take place

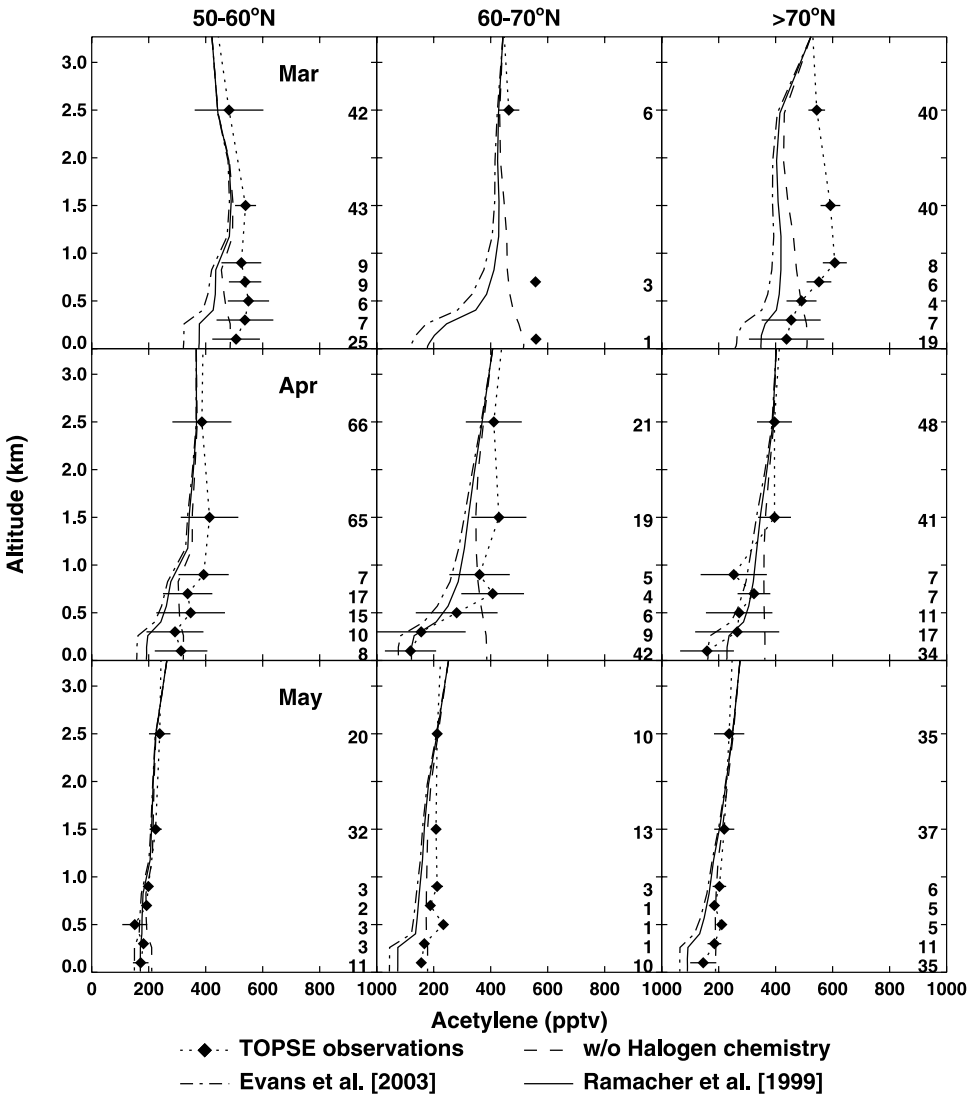

Figure 7c. Same as Figure 7a but for acetylene.

[e.g., *Koop et al.*, 2000]. Additional uncertainties could come from the mass accommodation coefficients and their temperature dependence [e.g., *Waschewsky and Abbatt*, 1999]. Similar kinetic uncertainties also exist for HOBr uptake.

[46] In addition to its photolysis, the destruction of Cl_2 can take place on a quasi-liquid surface [*Hu et al.*, 1995; *Mochida et al.*, 1998; *Adams et al.*, 2002]. Although the chemical mechanism used by *Evans et al.* [2003] is adopted from *Michalowski et al.* [2000], two aqueous-phase reactions, $Cl_2 + Br^- \rightarrow BrCl_2^-$ and $BrCl_2^- \rightarrow BrCl + Cl^-$, are not considered. The surface uptake of Cl_2 may effectively reduce Cl_2 concentrations to obtain a better Br/Cl estimate as shown by *Spicer et al.* [2002]. The quantitative effect cannot be evaluated in the present study.

[47] Using the empirical Cl/Br function by *Ramacher et al.* [1999], we test the sensitivity of the NMHC simulations to the thickness of the halogen layer. Ozone concentrations are much more sensitive to the assumed thickness of the halogen layer because of the quadratic dependence of ozone loss on BrO concentrations. Table 3 and Figure 8 show that effect of Cl oxidation does not strongly depend on the assumed thickness. The changes of the slope do not always monotonically increase with the decrease of the thickness of the halogen layer because of the effects of turbulence mixing and transport. The integrated halogen oxidations diagnosed using equations (11) and (12) reflect chemical processing and mixing of the air mass in previous days.

[48] The integrated Br oxidation represented by the deviation of acetylene from the least squares fit line is simulated well in the standard model for the first three flights but significantly underestimated in flight 34. Increasing the halogen layer thickness to 400 m does not significantly change the model results but decreasing the thickness by 100 m leads to much larger Br oxidation. At a thickness of 200 m, simulated ozone concentrations decrease to unrealistic low levels compared to the observa-

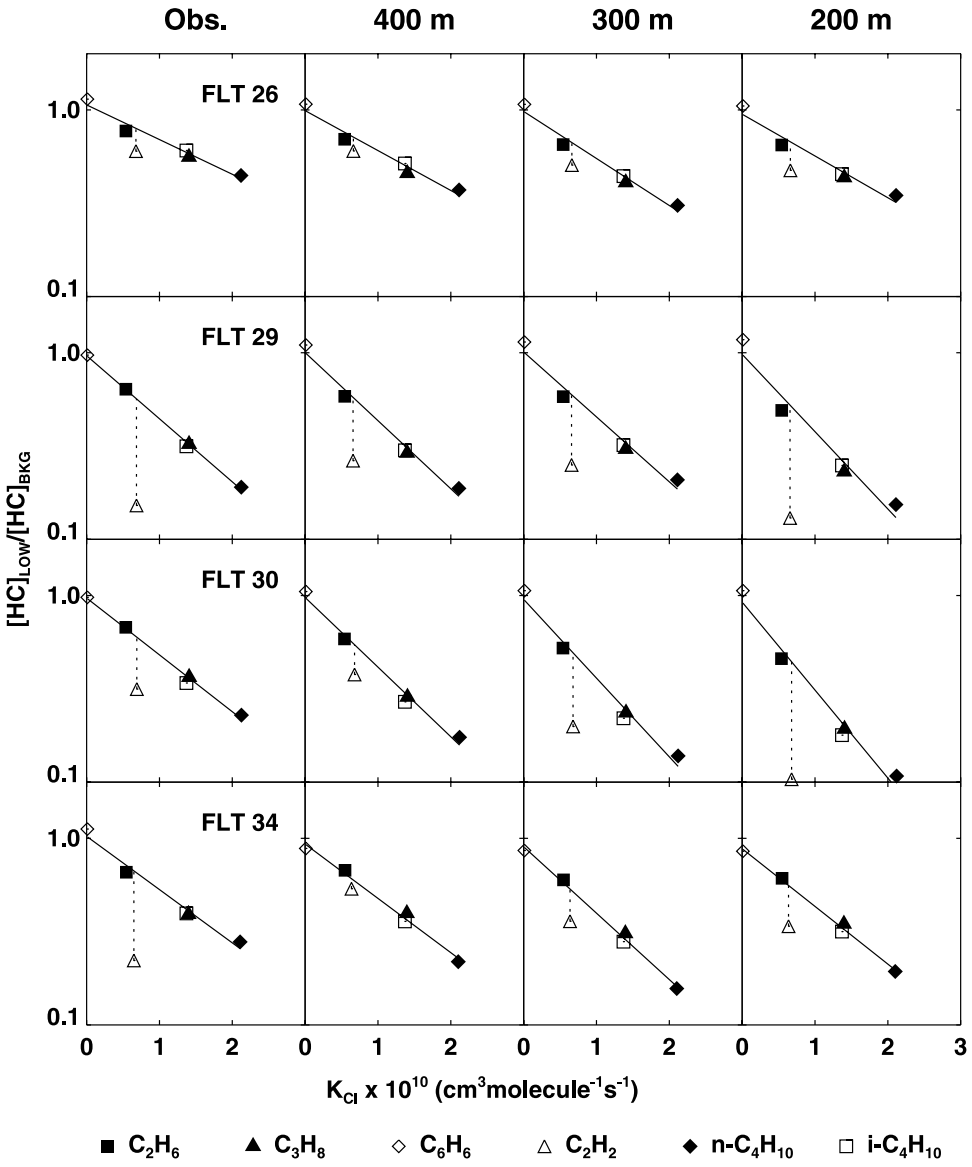

Figure 8. Differential NMHC losses by Cl and Br oxidation as a function of their reaction rate constant with Cl atom for four selected flights (see text for details). Model simulations using the empirical relationship of Br/Cl ratio by *Ramacher et al.* [1999] are conducted with the thickness of the halogen layer at 200, 300, and 400 m. The line represents a least squares fit through alkane and benzene data points. The slope values are listed in Table 3.

tions. Ozone concentrations tend to be underestimated in these flights in the standard model with a halogen layer thickness of 300 m but overestimated at 400 m. Therefore a typical thickness of 300–400 m for the halogen layer is consistent with the observations of aircraft measurements of ozone and NMHCs and surface ozone at Alert and Barrow. The sensitivity of low-altitude ozone to the BrO layer thickness is much higher than hydrocarbons because the

Table 3. Slope Values of the Least Squares Fits Shown in Figure 8

		Model Simulations			
	Observations	400 m[a]	300 m[a]	200 m[a]	300 m[b]
Flight 26	−0.43	−0.49	−0.58	−0.52	−1.18
Flight 29	−0.78	−0.84	−0.80	−0.95	−0.77
Flight 31	−0.70	−0.86	−0.97	−1.08	−0.94
Flight 34	−0.66	−0.67	−0.82	−0.71	−1.26

[a]Height of BrO layer in the simulations using Br/Cl ratios according to equation (10) based on the work by *Ramacher et al.* [1999].
[b]Height of BrO layer in the simulations using Br/Cl ratios based on the calculation by *Evans et al.* [2003].

dependence of ozone loss on BrO is quadratic while the loss of hydrocarbons to Cl or Br oxidation is linear.

5. Conclusions

[49] We applied a regional 3-D chemical transport model to simulate halogen-driven losses of ozone and NMHCs at northern high latitudes in spring, 2000. The polar version of NCAR/Penn State MM5 is used for meteorological data assimilation with the NCEP reanalysis and surface and rawinsonde observations. GOME observations of BrO column are used to specify the BrO concentrations in the model. The model simulations are evaluated using TOPSE in situ observations of ozone and NMHCs and surface ozone measurements at Alert and Barrow.

[50] GOME observations show large areas of high tropospheric BrO concentrations at northern high latitudes, which peak in March. The corresponding model simulations show widespread ozone loss, peaking instead in April because of increasing photochemical processing from the equinox to solstice. Over three selected high-BrO regions during the 4-month period, we find a clear anticorrelation between tropospheric GOME BrO column and assimilated surface temperature. The temporal phase change of BrO columns coincides with the movement of cold polar air masses. The variation of temperature, rather than the absolute value, appears to play a critical role in the activation and cycling of halogen radicals.

[51] The evaluation of model simulations with aircraft and surface observations generally demonstrates good agreement. We focus the discussion here on the model uncertainties. The model simulation of surface ozone for Barrow is better than for Alert. The more variable wind direction at Alert reflects a more complex geographical setting of the site than Barrow, a complexity not captured by the model. At a site like Alert where simulated low ozone concentrations are due almost exclusively to transport of poor ozone air from high-BrO regions, the quality of simulated transport is reflected directly in the resulting ozone simulations.

[52] Another large uncertainty in the model simulation is the calculation of Cl/Br ratio. We apply in the model two formulations of Cl/Br ratio as a function of ozone, one based on the empirical relationship derived from previous observations by *Ramacher et al.* [1999] and the other theoretical calculation using a box model with the currently accepted halogen mechanism [*Evans et al.*, 2003]. The theoretical formulation predicts higher Cl/Br ratios than the empirical one. The model simulations using the empirical formulation are in reasonably good agreement with observed vertical profiles of NMHCs and the diagnosed integrated Cl and Br oxidation based on the observed differential NMHC losses during selected flights with large ODEs. The model overestimates the Cl oxidation when using the theoretical formulation. The overestimation, which is modulated by the effects of transport and mixing, can be very large. There are large uncertainties in the kinetics parameters for the reaction of $HOCl + Cl^- + H^+ \rightarrow Cl_2 + H_2O$, including the strong temperature dependence of the rate constant, Henry's law constant in the quasi-liquid surface layer of aerosols or ice/snow, and the mass accommodation coefficient. Two additional aqueous-phase reactions, $Cl_2 + Br^- \rightarrow BrCl_2^-$ and $BrCl_2^- \rightarrow BrCl + Cl^-$ apparently not considered by *Evans et al.* [2003], can potentially be important in decreasing simulated Cl/Br ratios [e.g., *Spicer et al.*, 2002].

[53] A third uncertainty in the model simulation is the specified thickness of the halogen layer in addition to the uncertainty in GOME BrO retrievals. Ozone simulations are particularly sensitive to this parameter because of the quadratic dependence of ozone loss on BrO concentrations. Without direct measurements, we use ozone and NMHC simulations to evaluate the parameter. On the basis of the surface observations at Alert and Barrow, the best estimate of the thickness is 300 m. Using this estimate, the model is able to reproduce largely the observed ozone decrease toward the surface starting at 1 km due to vertical transport of ozone-poor air from low altitude, although there are a few occasions when the simulated ozone decrease starts at a lower altitude. The simulations of NMHCs are not as sensitive because the loss is linearly dependent on Cl or Br concentrations. The comparisons of simulated vertical profiles of NMHCs with the observations show consistent results with the ozone comparison; that is, the halogen-driven loss starts at about 1 km even though the thickness of the halogen layer is 300 m. Further investigation of four specific flights, which encountered large ozone losses, suggests that the average halogen layer thickness is 300–400 m. On the other hand, for the purpose of evaluating satellite BrO observations, using NMHCs observations is more robust than those of ozone because the simulation results are less sensitive to the specified thickness of the halogen layer.

[54] **Acknowledgments.** This work was supported by the National Science Foundation Atmospheric Chemistry Program. We thank Kurt Anlauf and Doug Worthy from Environment Canada for providing the ozone and meteorological data at Alert, Canada. The GEOS-CHEM model is managed at Harvard University with support from the NASA Atmospheric Chemistry Modeling and Analysis Program; we thank Robert Yantosca and Daniel Jacob for providing us the model and data. Last, we thank Darin Toohey and two anonymous reviewers for their insightful reviews and suggestions.

References

Adams, J. W., N. S. Holmes, and J. N. Crowley (2002), Uptake and reaction of HOBr on frozen and dry NaCl/NaBr surfaces between 253 and 233K, *Atmos. Chem. Phys.*, *2*, 79–91.

Anlauf, K., R. Mickle, and B. Trivett (1994), Measurement of ozone during Polar Sunrise Experiment 1992, *J. Geophys. Res.*, *99*, 25,345–25,353.

Ariya, P. A., et al. (1998), Measurements of C_2-C_7 hydrocarbons during the polar sunrise Experiment 1994: Further evidence for halogen chemistry in the troposphere, *J. Geophys. Res.*, *103*, 13,169–13,180.

Atkinson, R., and S. M. Aschmann (1985), Kinetics of the gas-phase reactions of Cl atoms with a series of organics at 296 ± 2 K and atmospheric pressure, *Int. J. Chem. Kinet.*, *17*, 33–41.

Atkinson, R., et al. (2002), Summary of evaluated kinetic and photochemical data for atmospheric chemistry, IUPAC Subcomm. on Gas Kinet. Data Eval. for Atmos. Chem., Research Triangle Park, N. C. (Available at http://www.iupac-kinetic.ch.cam.ac.uk/)

Atlas, E. L., B. A. Ridley, and C. A. Cantrell (2003), The Tropospheric Ozone Production about the Spring Equinox (TOPSE) Experiment: Introduction, *J. Geophys. Res.*, *108*(D4), 8353, doi:10.1029/2002JD003172.

Barrie, L. A., J. W. Bottenheim, R. C. Schnell, P. J. Crutzen, and R. A. Rasmussen (1988), Ozone destruction and photochemical reactions at polar sunrise in the lower Arctic atmosphere, *Nature*, *334*, 138–141.

Bey, I., et al. (2001), Global modeling of tropospheric chemistry with assimilated meteorology: Model description and evaluation, *J. Geophys. Res.*, *106*, 23,073–23,096.

Bierbach, A., I. Barnes, and K. H. Becker (1999), Rate constants of the Br-initiated gas-phase oxidation of a series of alcohols, furans and benzenes at 300 ± 2 K, *Atmos. Environ.*, *33*, 2981–2992.

Blake, N. J., D. R. Blake, B. C. Sive, A. S. Katzenstein, S. Meinardi, O. W. Wingenter, E. L. Atlas, F. Flocke, B. A. Ridley, and F. S. Rowland (2003), The seasonal evolution of NMHCs and light alkyl nitrates at middle to high northern latitudes during TOPSE, *J. Geophys. Res.*, *108*(D4), 8359, doi:10.1029/2001JD001467.

Bottenheim, J. W., A. G. Gallant, and K. A. Brice (1986), Measurements of NO_y species and O_3 at 82°N latitude, *Geophys. Res. Lett.*, *13*, 113–116.

Boudries, H., and J. W. Bottenheim (2000), Cl and Br atom concentrations during a surface ozone depletion event in the Canadian high Arctic, *Geophys. Res. Lett.*, *27*, 517–520.

Bromwich, D. H., J. J. Cassano, T. Klein, G. Heinemann, K. M. Hines, K. Steffen, and J. E. Box (2001), Mesoscale modeling of katabatic winds over Greenland with the Polar MM5, *Mon. Weather Rev.*, *129*, 2290–2309.

Browell, E. V., et al. (2003), Ozone, aerosol, potential vorticity, and trace gas trends observed at high-latitudes over North America from February to May 2000, *J. Geophys. Res.*, *108*(D4), 8369, doi:10.1029/2001JD001390.

Cassano, J. J., J. E. Box, D. H. Bromwich, L. Li, and K. Steffen (2001), Evaluation of Polar MM5 simulations of Greenland's atmospheric circulation, *J. Geophys. Res.*, *106*, 33,867–33,889.

Chance, K. (1998), Analysis of BrO measurements from the Global Ozone Monitoring Experiment, *Geophys. Res. Lett.*, *25*, 3335–3338.

Choi, Y., Y. Wang, T. Zeng, R. V. Martin, T. P. Kurosu, and K. Chance (2005), Evidence of lightning NO_x and convective transport of pollutants in satellite observations over North America, *Geophys. Res. Lett.*, *32*, L02805, doi:10.1029/2004GL021436.

European Space Agency (1985), *The GOME Users Manual*, edited by F. Bednarz, *European Space Agency Spec. Publ. ESA SP-1182*. (Available at http://earth.esa.int/services/esa_doc/doc_gom.html)

Evans, M. J., et al. (2003), Coupled evolution of BrO_x-ClO_x-HO_x-NO_x chemistry during bromine-catalyzed ozone depletion events in the arctic boundary layer, *J. Geophys. Res.*, *108*(D4), 8368, doi:10.1029/2002JD002732.

Fan, S. M., and D. J. Jacob (1992), Surface ozone depletion in Arctic spring sustained by bromine reactions on aerosols, *Nature*, *359*, 522–524.

Fitzenberger, R., et al. (2000), First profile measurements of tropospheric BrO, *Geophys. Res. Lett.*, *27*, 2921–2924.

Foster, L. L., et al. (2001), The role of Br_2 and BrCl in the surface ozone destruction at polar sunrise, *Science*, *291*, 471–474.

Gautrois, M., T. Brauers, R. Koppmann, F. Rohrer, O. Stein, and J. Rudolph (2003), Seasonal variability and trends of volatile organic compounds in the lower polar troposphere, *J. Geophys. Res.*, *108*(D13), 4393, doi:10.1029/2002JD002765.

Gong, S. L., J. L. Walmsley, L. A. Barrie, and J. F. Hopper (1997), Mechanisms for surface ozone depletion and recovery during polar sunrise, *Atmos. Environ.*, *31*, 969–981.

Hausmann, M., and U. Platt (1994), Spectroscopic measurement of bromine oxide and ozone in the high Arctic during Polar Sunrise Experiment 1992, *J. Geophys. Res.*, *99*, 25,399–25,413.

Hu, J. H., et al. (1995), Reactive uptake of Cl_2 (g) and Br_2 (g) by aqueous surfaces as a function of Br- and I-ion concentration: The effect of chemical reaction at the interface, *J. Phys. Chem.*, *99*, 8768–8776.

Impey, G. A., et al. (1999), Measurements of photolyzable halogen compounds and bromine radicals during the Polar Sunrise Experiment 1997, *J. Atmos. Chem.*, *34*, 21–37.

Jobson, B. T., et al. (1994), Measurements of C_2-C_6 hydrocarbons during the polar sunrise 1992 experiment: Evidence for Cl atom and Br atom chemistry, *J. Geophys. Res.*, *99*, 25,355–25,368.

Kaleschke, L., et al. (2004), Frost flowers on sea ice as a source of sea salt and their influence on tropospheric halogen chemistry, *Geophys. Res. Lett.*, *31*, L16114, doi:10.1029/2004GL020655.

Koop, T., A. Kapilashrami, L. T. Molina, and M. J. Molina (2000), Phase transitions of sea-salt/water mixtures at low temperatures: Implications for ozone chemistry in the polar marine boundary layer, *J. Geophys. Res.*, *105*, 26,393–26,402.

Lay, T. H., J. W. Bozzelli, and J. H. Seinfeld (1996), Atmospheric photochemical oxidation of benzene: Benzene plus OH and the benzene-OH adduct (hydroxy-2,4-cyclohexadienyl) plus O_2, *J. Phys. Chem.*, *100*, 6543–6554.

Madronich, S., and S. Flocke (1998), The role of solar radiation in atmospheric chemistry, in *Handbook of Environmental Chemistry*, edited by P. Boule, pp. 1–26, Springer, New York.

Martin, R. V., et al. (2002), An improved retrieval of tropospheric nitrogen dioxide from GOME, *J. Geophys. Res.*, *107*(D20), 4437, doi:10.1029/2001JD001027.

McConnell, J. C., et al. (1992), Photochemical bromine production implicated in Arctic boundary layer ozone depletion, *Nature*, *355*, 150–152.

McElroy, C. T., C. A. McLinden, and J. C. McConnell (1999), Evidence for bromine monoxide in the free troposphere during the Arctic polar sunrise, *Nature*, *397*, 338–341.

Michalowski, B., et al. (2000), A computer model study of multiphase chemistry in the Arctic boundary layer during polar sunrise, *J. Geophys. Res.*, *105*, 15,131–15,145.

Middleton, P., W. R. Stockwell, and W. P. L. Carter (1990), Aggregation and analysis of volatile organic compound emissions for regional modeling, *Atmos. Environ., Part A*, *24*, 1107–1133.

Mochida, M., J. Hirokawa, Y. Kajii, and H. Akimoto (1998), Heterogeneous reactions of Cl_2 with sea salts at ambient temperature: Implications for halogen exchange in the atmosphere, *Geophys. Res. Lett.*, *25*, 3927–3930.

Oltmans, S. J., and H. Levy II (1994), Surface ozone measurements from a global network, *Atmos. Environ.*, *28*, 9–24.

Oltmans, S. J., et al. (1986), Surface ozone distributions and variations from 1973–1984 measurements at the NOAA geophysical monitoring for climatic change baseline observatories, *J. Geophys. Res.*, *91*, 5236–5299.

Piccot, S. D., J. J. Watson, and J. W. Jones (1992), A global inventory of volatile organic compound emissions from anthropogenic sources, *J. Geophys. Res.*, *97*, 9897–9912.

Platt, U., and C. Janssen (1995), Observation and role of the free radicals NO_3, ClO, BrO and IO in the troposphere, *Faraday Disc.*, *100*, 175–198.

Ramacher, B., J. Rudolph, and R. Koppmann (1999), Hydrocarbon measurements during tropospheric ozone depletion events: Evidence for halogen atom chemistry, *J. Geophys. Res.*, *104*, 3633–3653.

Rankin, A. M., E. W. Wolff, and S. Martin (2002), Frost flowers: Implications for tropospheric chemistry and ice core interpretation, *J. Geophys. Res.*, *107*(D23), 4683, doi:10.1029/2002JD002492.

Richter, A., F. Wittrock, M. Eisinger, and J. P. Burrows (1998), GOME observations of tropospheric BrO in Northern Hemispheric spring and summer 1997, *Geophys. Res. Lett.*, *25*, 2683–2686.

Ridley, B. A., et al. (2003), Ozone depletion events observed in the high latitude surface layer during the TOPSE aircraft program, *J. Geophys. Res.*, *108*(D4), 8356, doi:10.1029/2001JD001507.

Sander, R., and P. J. Crutzen (1996), Model study indicating halogen activation and ozone destruction in polluted air masses transported to the sea, *J. Geophys. Res.*, *101*, 9121–9138.

Sander, R., R. Vogt, G. W. Harris, and P. Crutzen (1997), Modeling the chemistry of ozone, halogen compounds, and hydrocarbons in the Arctic troposphere during spring, *Tellus, Ser. B*, *49*, 522–532.

Sander, S. P., et al. (2003), Chemical kinetics and photochemical data for use in atmospheric studies, evaluation 14, *JPL Publ.*, *02-25*, NASA Jet Propul. Lab., Pasadena, Calif.

Sokolov, O., et al. (1998), Kinetics and mechanism of the gas-phase reaction of Cl atoms with benzene, *J. Phys. Chem. A*, *102*, 10,671–10,681.

Solberg, S., N. Schmidtbauer, A. Semb, and F. Stordal (1996), Boundary-layer ozone depletion as seen in the Norwegian Arctic in spring, *J. Atmos. Chem.*, *23*, 301–332.

Spicer, C. W., et al. (2002), Molecular halogens before and during ozone depletion events in the Arctic at polar sunrise: Concentrations and sources, *Atmos. Environ.*, *36*, 2721–2731.

Sumner, A. L., and P. B. Shepson (1999), Snowpack production of formaldehyde and its effect on the Arctic troposphere, *Nature*, *398*, 230–233.

Tang, T., and J. C. McConnell (1996), Autocatalytic release of bromine from Arctic snow pack during polar sunrise, *Geophys. Res. Lett.*, *19*, 2633–2636.

Tarasick, D. W., and J. W. Bottenheim (2002), Surface ozone depletion episodes in the Arctic and Antarctic from historical ozonesonde records, *Atmos. Chem. Phys.*, *2*, 197–205.

Tuckermann, M., et al. (1997), DOAS-observation of halogen radical-catalysed arctic boundary layer ozone destruction during the ARCTOC-campaigns 1995 and 1996 in Ny-Ålesund, Spitsbergen, *Tellus, Ser. B*, *49*, 533–555.

Vogt, R., P. J. Crutzen, and R. Sander (1996), A mechanism for halogen release from the sea-salt aerosol in the remote marine boundary layer, *Nature*, *383*, 327–330.

Wagner, T., and U. Platt (1998), Satellite mapping of enhanced BrO concentrations in the troposphere, *Nature*, *395*, 486–489.

Wagner, T., C. Leue, M. Wenig, K. Pfeilsicker, and U. Platt (2001), Spatial and temporal distribution of enhanced boundary layer BrO concentrations measured by the GOME instrument aboard ERS-2, *J. Geophys. Res.*, *106*, 24,225–24,235.

Wang, T. X., and D. W. Margerum (1994), Kinetics of reversible chlorine hydrolysis: Temperature dependence and general-acid/base-assisted mechanisms, *Inorg. Chem.*, *33*, 1050–1055.

Wang, Y., and T. Zeng (2004), On tracer correlations in the troposphere: The case of ethane and propane, *J. Geophys. Res.*, *109*, D24306, doi:10.1029/2004JD005023.

Wang, Y., D. Jacob, and J. A. Logan (1998), Global simulation of tropospheric O_3-NO_x-hydrocarbon chemistry: 1. Model formulation, *J. Geophys. Res.*, *103*, 10,713–10,726.

Wang, Y., et al. (2003a), Intercontinental transport of pollution manifested in the variability and seasonal trend of springtime O_3 at northern middle and high latitudes, *J. Geophys. Res.*, *108*(D21), 4683, doi:10.1029/2003JD003592.

Wang, Y., et al. (2003b), Springtime photochemistry at northern mid and high latitudes, *J. Geophys. Res.*, *108*(D4), 8358, doi:10.1029/2002JD002227.

Warneck, P. (1999), *Chemistry of the Natural Atmosphere*, 2nd ed., Elsevier, New York.

Waschewsky, G. C. G., and J. P. D. Abbatt (1999), HOBr in sulfuric acid solutions: Solubility and reaction with HCl as a function of temperature and concentration, *J. Phys. Chem. A*, *103*, 5312–5320.

Zeng, T. (2005), Three-dimensional model analysis of tropospheric photochemical processes in the Arctic and northern mid-latitudes, Ph.D. thesis, Ga. Inst. of Technol., Atlanta.

Zeng, T., Y. Wang, K. Chance, E. V. Browell, B. A. Ridley, and E. L. Atlas (2003), Widespread persistent near-surface ozone depletion at northern high latitudes in spring, *Geophys. Res. Lett.*, *30*(24), 2298, doi:10.1029/2003GL018587.

D. Blake and N. Blake, Department of Chemistry, University of California, Irvine, CA 92697, USA.

K. Chance, Harvard-Smithsonian Center for Astrophysics, Cambridge, MA 02138, USA.

B. Ridley, Atmospheric Chemistry Division, National Center for Atmospheric Research, Boulder, CO 80307, USA.

Y. Wang and T. Zeng, School of Earth and Atmospheric Sciences, Georgia Institute of Technology, Atlanta, GA 30332, USA. (tzeng@eas.gatech.edu)